ICARUS 54, 296–308 (1983)

Saturn Meteorology: A Diagnostic Assessment of Thin-Layer Configurations for the Zonal Flow[1]

MICHAEL ALLISON*,[2] AND PETER H. STONE†

*NASA Goddard Space Flight Center, Institute for Space Studies, 2880 Broadway, New York, New York 10025, and †Department of Meteorology and Physical Oceanography, Massachusetts Institute of Technology, Cambridge, Massachusetts 02139

Received August 30, 1982; revised December 15, 1982

Voyager imaging, infrared, and radio observations for Saturn have been recently interpreted by Smith *et al.* (1982) as an indication that the jet streams observed at the cloud tops extend to depths greater than the 10^4-bar level. This analysis assumes a maximum latitudinal temperature contrast of a few percent, a mean atmospheric rotation rate at depth given by Saturn's ratio period, and no variation with latitude of the bottom pressure level for the zonal flow system. These assumptions are not, however, firmly constrained by observation. The diagnostic analysis of plausible alternative configurations for Saturn's atmospheric structure demonstrates that a thin weather layer system (confined at mid to high latitudes to levels above 200 bar) cannot be excluded by any of the available observations. A quantitative estimate of the effects of moisture condensation (including the differentiation of mean molecular weight) suggests that these might provide the buoyancy contrasts necessary to support a thin-layer flow provided that Saturn's outer envelope is enriched approximately 10 times in water abundance relative to a solar composition atmosphere and strongly differentiated with latitude at the condensation level.

INTRODUCTION

The atmospheric dynamics of Saturn and Jupiter remain a formidable challenge to theoretical understanding. Both planets show strongly super-rotating equatorial currents and at higher latitudes an axisymmetric and long-lived pattern of alternating westward and eastward jet streams. On Saturn, however, the currents are somewhat stronger, wider in latitudinal extent, and more dominantly prograde, measured with respect to the planet's ratio period, than for Jupiter (Smith *et al.*, 1982).

Two extreme pictures of the global scale dynamics for the Jovian planets have emerged. In one view, the wind patterns are the observed effect of interior convection organized into multiple counter-rotating cylinders, concentric with the planetary spin axis, and extending through the bulk of the molecular hydrogen envelope (Busse, 1976; Ingersoll and Pollard, 1982). In the other view the observed zonal flow is confined to a thin upper weather layer with a small vertical to horizontal aspect ratio (e.g., Conrath *et al.*, 1981), possibly supported by differential radiative absorption and phase changes associated with the condensation of atmospheric constituents (Gierasch, 1976). Both pictures of the Jovian dynamics thus far lack a complete theory which can satisfactorily account for all the observations.

Recently, however, Smith *et al.* (1982) have suggested that the Voyager imaging, infrared, and radio observations for Saturn together imply that the flow patterns at the cloud tops must extend to depths greater than the 10^4-bar level and that thin-layer models for both Saturn and Jupiter must be reexamined with this conclusion in mind. We will review the observational and theoretical assumptions of this analysis and show that the stated conclusion is quite sensitive to the adopted parameter settings.

[1] Paper presented at the "Saturn Conference," Tucson, Arizona, May 11–15, 1982.

[2] To whom correspondence should be addressed.

0019-1035/83 $3.00

A generalized diagnostic analysis of plausible alternative configurations for Saturn's dynamic atmosphere suggests that a thin weather layer geometry is still consistent with all the available observations. We present and discuss a few numerical examples of previously neglected effects which might be of controlling importance for the dynamical balance of a thin-layer flow system on Saturn. The indicated depth for the zonal flow in these examples is between 50 and 200 bar. While we will argue that it is too early to exclude an entire class of Jovian atmospheric models, we acknowledge that the work of Smith *et al.* (1982) has led us to expect that the flow may well lie at deeper levels on Saturn than such models have previously assumed.

OBSERVATIONAL CONSTRAINTS

Smith *et al.* (1982) present measurements of Saturn's zonal velocity as inferred from the drift rates of cloud features (in the vicinity of the 350-mb level). A smooth fit to their published data is indicated by the solid curve in Fig. 1. These cloudtop velocities

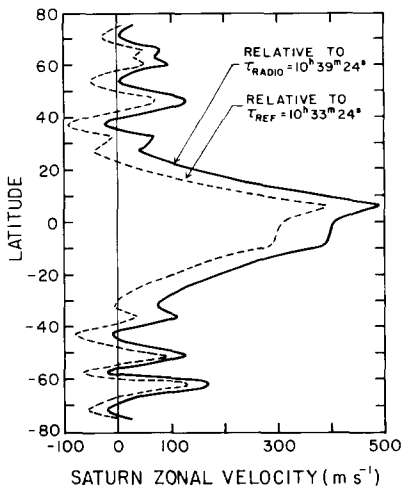

FIG. 1. Saturn zonal wind velocity at the cloudtop level inferred from Voyager imaging measurements. The solid curve represents a smooth fit to the data of Smith *et al.* (1982) measured with reference to Saturn's radio period. The dashed curve corresponds to the same measurements in a frame of reference with a rotational period 6 min less than that of the radio period.

are computed with reference to the measured Saturn radio period τ_{radio} as

$$u_T'(\lambda) = 2\pi a[\tau_f^{-1}(\lambda) - \tau_{radio}^{-1}]\cos\lambda, \quad (1)$$

where a denotes the planetary radius and τ_f the rotation period of a tracked cloud feature at latitude λ. (Here we neglect a small correction in the rotation radius of features due to the planet's oblateness which does not significantly affect the following diagnostic analysis.)

The wind profile derived in this way may be expected to indicate the velocity of cloudtop motions with respect to the bulk of the planet provided that the deep interior rotates as a solid body at the same rate as the radio period. It is possible, however, that the bulk interior of Saturn does not rotate at exactly the measured radio period. This possibility is mentioned by Smith *et al.* (1982) and bears consideration as a potentially important effect on the diagnostic analysis of the draft rates.

The radio period associated with Saturn's kilometric radiation has been accurately measured by Desch and Kaiser (1981) as $\tau_{radio} = 10^h39^m24^s$ to within $\pm 7^s$. The strength of the kilometric signal, however, is sporadic and unexpectedly modulated by the planet's rotation, with preferential emission occurring when Saturn has a particular phase relative to the Sun (Warwick *et al.*, 1981). Kaiser *et al.* (1981) have analyzed the beam geometry of the kilometric radiation and have inferred that the source of the radio signal is probably tied to a northern high-latitude sector of the auroral zone at a longitude close to the local noon meridian. (They note that this region is a good candidate for the enhanced particle precipitation required to produce the radio emission.) If this region is in fact the source of the signal and if its rotation or emission period is shifted with respect to the rotation of the deep interior of the planet, then the motion of the cloud-tracked features with respect to the interior will assume a character different from that of the solid curve of Fig. 1.

We do not attempt to suggest how such a frequency shift between the signal-generating sector and the deep interior core might be expected to occur but will explore the effects of a 1% change in the reference rotation period on the dynamical analysis of the cloudtop winds. Solving Eq. (1) for τ_f^{-1} and back-substituting the result with τ_{radio} replaced by some other reference period τ_{ref} we obtain the cloudtop velocity in the new frame as

$$u_T(\lambda) = u'_T(\lambda) + 2\pi a[\tau_{radio}^{-1} - \tau_{ref}^{-1}]\cos\lambda. \quad (2)$$

The dashed curve in Fig. 1 shows the zonal velocity thus computed from the published drift speeds with reference to a rotation period which is 6 min shorter than the measured radio signal. In this frame of reference, the high-latitude jet streams assume a periodic variation between eastward and westward flow more like that inferred for Jupiter. (cf. Fig. 2 of Ingersoll *et al.*, 1981). We emphasize that the dashed profile in Fig. 1 is only one example of how the real motion with respect to the interior might differ from the published result, owing to the uncertainty about the exact connection between the interior magnetic field and the observed radio signal.

The other observational constraint invoked by Smith *et al.* (1982) in their dynamical analysis of the zonal flow comes from the Voyager infrared interferometer spectrometer (or IRIS) observations. They infer from published data a maximum equator to pole temperature variation of 2%. They also estimate a maximum mean molecular weight variation with latitude of 2% to yield a maximum combined variation of 4% in the virtual temperature of the zonal flow layer between equator and pole.

Figure 2 presents a zonally averaged thermal cross section of the deviation from the latitudinal mean retrieved temperature at each indicated pressure level in Saturn's northern hemisphere obtained by Voyager 1 IRIS and published by Pirraglia *et al.* (1981). They caution that retrievals below 300 mb may be affected by variable haze concentration (cf. Conrath and Pirraglia, 1982). In fact, recent work by West (1983) indicates that unit optical depths at visible wavelengths in Saturn's atmosphere lie between 200 and 500 mb. Figure 2 does suggest, however, that the global thermal contrasts between low and high latitudes above 300 mb may be as large as 10°K, or roughly 12% of the retrieved upper tropospheric temperature (≈86°K), and in the sense expected for differential solar driving.

The structure shown in the upper part of the cross section may well include a transient component associated with the northern winter season. (Although the Voyager arrived at Saturn shortly after the Spring equinox, the radiative time constant at these upper atmospheric levels is comparable to the Saturnian year.) Measurements for Saturn's southern hemisphere are more sparsely placed than those used in the construction of Fig. 2 but do show less latitudinal contrast (Conrath and Pirraglia, 1982). If the contrasts shown in Fig. 2 are in fact partly seasonal, then the view that differential solar heating is operative at these levels is only reinforced.

At greater depths below the cloudtops the radiative lag time is longer than the Saturnian year and seasonal effects will tend to be suppressed. (The time constants may be estimated from the work of Gierasch and Goody, 1969.) The radiative response of the

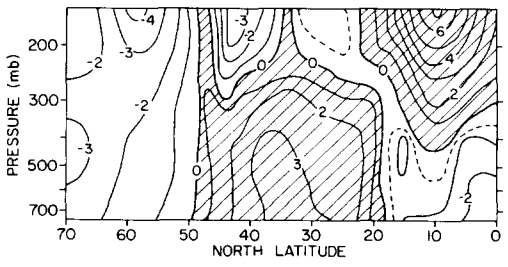

FIG. 2. Zonally averaged cross section of the deviation from the latitudinal mean retrieved temperature (°K) at each indicated pressure level in Saturn's northern hemisphere from Voyager 1 IRIS measurements (after Pirraglia *et al.*, 1981). Reprinted by permission from *Nature*, Vol. **292,** No. 5825, pp. 677–679. Copyright © 1981 Macmillan Journals Limited.

cloud layer may then be controlled by the yearly mean of the differential heating between equator and pole so that all hemispheric asymmetries as well as seasonal changes would be absent at these levels. Thus, the IRIS observations are in no way inconsistent either with differential heating of the cloud layer below 350 mb or with the imaging observations of the hemispheric symmetry of the jets (cf. Fig. 1).

Ingersoll (1976) has proposed that the planet's internal convection may compensate for the differential solar heating in a way which could severely limit the magnitude of latitudinal temperature contrasts. Other theoretical pictures for the convective transport of the internal heat through the upper cloud zone are possible, however, with large circulation cells taking the place of small scale eddies (cf. Gierasch, 1976). The real situation depends upon the vertical structure of the atmosphere at levels where we have little or no information. Further work with radiative–convective models is needed to assess the possible differential heating at subcloud levels by the absorption of sunlight.

The most important point to be made here is that there is no purely observational basis for firmly restricting the equator-to-pole thermal contrast below the cloud deck, whatever its source, to 4%. It is worth noting that on the Earth the latitudinal thermal gradients measured at upper tropospheric levels are significantly weaker than those at lower altitudes. (cf. COSPAR, 1972.)

GEOPOTENTIAL ANALYSIS

Smith *et al.* (1982) apply the observed drift rates on Saturn to an analysis of the geopotential height variation with depth and latitude. We repeat this analysis in somewhat greater generality to examine the continuous dependence of the required bottom pressure upon the latitudinal thermal contrast and to allow for the possibility that the bottom pressure for the flow may itself vary with latitude.

The geopotential is just the effective gravitational potential at some elevation z as compared with some reference elevation z_0. That is,

$$\Phi = \int_{z_0}^{z} g dz, \tag{3}$$

where g denotes the effective gravitational acceleration (corrected for the local centrifugal acceleration). In the absence of any topographic structure, it is convenient to express vertical variations within the atmosphere in terms of the nondimensional pressure $\zeta \equiv p/p_T$, where p_T denotes the pressure at the cloudtop level, and to take horizontal gradients along isobaric surfaces. For a convective atmosphere, it is also convenient to employ the potential temperature function Θ defined with respect to the ordinary temperature T according to $\Theta = T\zeta^{-R/c_p}$, where R is the gas constant and c_p the specific heat at constant pressure.

Recent work by Massie and Hunten (1982) suggests that *ortho–para* conversion of hydrogen catalyzed by the presence of aerosols in Jovian atmospheres may induce vertical variations in the specific heat at levels less deep than 5 bars. The dynamical consequences are investigated by Gierasch (1983). For the present analysis, we adopt the classical ratio of $R/c_p = 0.2937$ (assumed constant) where $R = 3.89 \times 10^7$ cm^2 s^{-2} K^{-1} for an atmosphere composed of 93% hydrogen and 7% helium by number fraction. (It is expected that these values will be obtained in the deep atmosphere where higher temperatures prohibit the conversion of quantum rotational states for the molecular hydrogen.) The assumed number fractions for hydrogen and helium are approximately consistent with those inferred from Voyager IRIS measurements for Saturn.

With the assumption of hydrostatic balance for an ideal gas the vertical variation of the geopotential is given as

$$\partial\Phi/\partial\zeta = -R\Theta\zeta^{R/c_p - 1}. \tag{4}$$

By the assumption of geostrophic balance the variation of Φ with latitude along an

isobaric surface is given in terms of the zonal velocity $u(\lambda,\zeta)$ according to

$$\partial\Phi/\partial\lambda = -2\Omega a u(\lambda,\zeta)\sin\lambda, \quad (5)$$

where Ω denotes the planetary rotation frequency.

Now Eq. (5) may be integrated at the cloudtop level using the data given in Fig. 1 to yield

$$\Delta\Phi'_T(\lambda) \equiv \Phi'(\lambda,1) - \Phi'(0,1) = -\int_0^\lambda 2\Omega a u'_T(\lambda)\sin\lambda d\lambda. \quad (6)$$

This integration has been carried out by Smith *et al.* (1982) for their velocity profile. In Fig. 3 we reproduce a plot of $\Delta\Phi'_T(\lambda)/c_p$ (in Kelvin units). The solid curve indicates the result of the integration over the zonal wind in the northern hemisphere measured with reference to the radio period. By replacing $u'_T(\lambda)$ in Eq. (6) with $u_T(\lambda)$ as given in Eq. (2) we may compute the latitudinal geopotential contrast for winds measured with respect to some other reference period τ_{ref} as

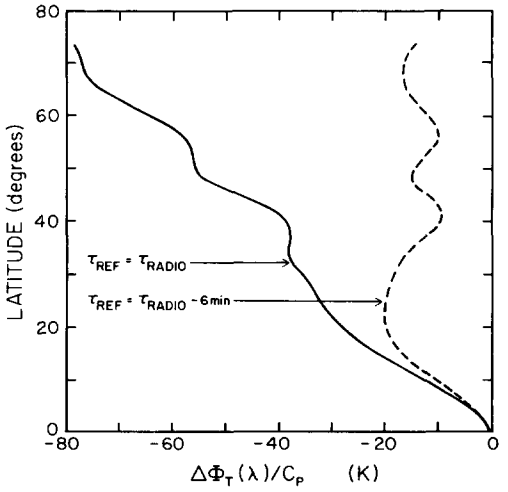

FIG. 3. Geopotential contrast with latitude at the cloudtop level, divided by c_p, as inferred from Voyager imaging measurements of wind velocities in Saturn's northern hemisphere. The solid curve corresponds to measurements with reference to the radio period, the dashed curve to measurements with reference to a period 6 min shorter than the radio period.

$$\Delta\Phi_T(\lambda) = \Delta\Phi'_T(\lambda) + 2\pi a^2\Omega(\tau_{radio}^{-1} - \tau_{ref}^{-1})\sin^2\lambda. \quad (7)$$

The result for $\tau_{ref} = \tau_{radio} - 6$ min, again divided by c_p, is given by the dashed curve in Fig. 3. In this case, the total latitudinal geopotential contrast between equator and pole is approximately four times smaller than that for the zonal winds in the frame of the radio period. Clearly, the meteorological analysis is very sensitive to small changes in the selection of the rotational reference frame.

Now the determination of the vertical variation of the geopotential height over the depth of the zonal flow from Eq. (4) requires the specification of the vertical variation of Θ. Because of Saturn's internal heating and associated convection, the thermal structure of the deep atmosphere is expected to be very nearly adiabitic (i.e., $\delta\Theta/\delta\zeta = 0$ at these levels). Equations (4) and (5) together imply the existence of a thermal wind shear (with pressure) wherever Θ varies with latitude. Thus if the zonal flow is to be confined to a thin upper layer, the potential temperature at lower levels may be expected to be independent not only of ζ but also of λ. (i.e., the lower layer will be approximately isentropic.) Although Θ will vary with latitude above the level of no motion we will assume, following Smith *et al.* (1982), that the vertical structure is nearly adiabatic there also. The large-scale motions are themselves unlikely to change this assumption (Stone, 1972, 1976). Unlike Smith *et al.* and other thin-layer studies, we will allow for the possibility that the no-motion level ζ_B may vary with latitude. In summary, we assume

$$\Theta(\lambda,\zeta) = \begin{cases} \Theta(\lambda) \text{ for } \zeta \le \zeta_B(\lambda) \\ \Theta_D, \text{ a constant, for } \zeta > \zeta_B(\lambda). \end{cases} \quad (8)$$

The indicated jump in potential temperature between levels above and below $\zeta_B(\lambda)$ might be more realistically represented as a continuous change in Θ induced over some thin but finite thickness by the radiative ab-

sorption or latent heating within a cloud layer. Another possibility is that cloud effects maintain a thermal structure which is significantly subadiabatic throughout the upper weather layer. We will, however, omit such considerations from the present diagnostic analysis.

The assumed structure is indicated schematically in Fig. 4. We emphasize that the variation of the bottom level ζ_B with latitude is included only as a possibility thus far unconstrained by any observation. Also, we note that no assumption is made in this analysis about the dynamic lower boundary condition for the weather layer. The vertical velocity at ζ_B is irrelevant to the diagnostic analysis of the motions provided that the zonal flow in the upper layer is geostrophic and the zonal flow in the lower layer is everywhere negligible by comparison. In a complete dynamical model, the vertical velocity might be of controlling importance in adjusting the latitudinal variation of the depth of the interface. Here we are only concerned with analyzing the necessary correlation between the assumed kinematic configuration and the geostrophic wind and temperature fields.

The terrestrial oceanic currents may offer a natural example of the type of configuration we consider here for Saturn. Both

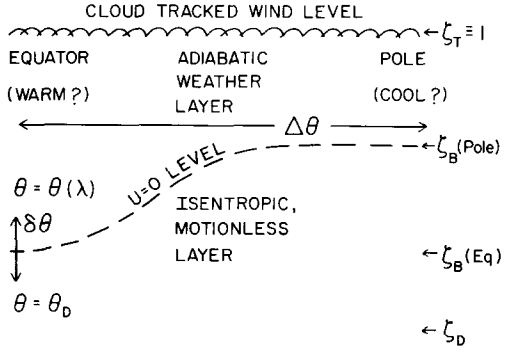

FIG. 4. Schematic diagram of the geometry of a thin zonal flow layer in Saturn's upper atmosphere. The dashed curve denotes the level of no zonal motion at the bottom of the upper zonal flow layer. See text for details.

systems show large scale geostrophic motion within a fluid which is weakly stratified at depth. Velocity sections of the ocean currents (see, for example, Fig. 24 of Nitani, 1972) show strong zonal motions confined to a thin layer (in the vicinity of the thermocline) with a lower level of no motion which varies strongly with latitude.

The vertical integration of the hydrostatic balance Eq. (4) at some fixed latitude for pressure levels between $\zeta_T \equiv 1$ and some deep level ζ_D greater than the maximum of $\zeta_B(\lambda)$ for all latitudes yields the relation

$$\Phi(\lambda,1) - \Phi(\lambda,\zeta_D) = c_p\{\Theta(\lambda)[\zeta_B{}^{R/c_p}(\lambda) - 1] + \Theta_D\,[\zeta_D{}^{R/c_p} - \zeta_B{}^{R/c_p}(\lambda)]\}. \quad (9)$$

Then, after taking the difference between the values for the last result evaluated at the pole and at the equator we obtain

$$[\Phi(P,1) - \Phi(E,1)]/c_p - [\Phi(P,\zeta_D) - \Phi(E,\zeta_D)]/c_p = \Theta_D[\zeta_B{}^{R/c_p}(E) - \zeta_B{}^{R/c_p}(P)] + \Theta(P)[\zeta_B{}^{R/c_p}(P) - 1] - \Theta(E)[\zeta_B{}^{R/c_p}(E) - 1], \quad (10)$$

where we have denoted the polar latitude by P and the equatorial latitude by E. The second term on the left side of this last equation is zero by the latitudinal integration of the geostrophic Eq. (4) along $\zeta = \zeta_D$, where the flow velocity is zero everywhere. The first term on the left has already been evaluated by Eq. (7) with the results displayed in Fig. 3 for two different choices of the reference period. It is convenient to define LGC $\equiv \Delta\Phi_T(P)/c_p$, the total latitudinal geopotential contrast at the cloudtops, and set

$$\delta\Theta \equiv \Theta(E) - \Theta_D, \quad (11)$$

and

$$\Delta\Theta \equiv \Theta(E) - \Theta(P), \quad (12)$$

(cf. Fig. 4). We may then rewrite the geopotential balance Eq. (10) as

$$\text{LGC} = \zeta_B{}^{R/c_p}(P)[\delta\Theta - \Delta\Theta] - \delta\Theta\zeta_B{}^{R/c_p}(E) + \Delta\Theta. \quad (13)$$

We now analyze the required balance of bottom pressure and thermal contrast for the Saturn weather layer by considering the following special cases for the parameter settings in Eq. (13).

Case 1. $\zeta_B(P) = \zeta_B(E)$. In this case, corresponding to a flat bottom for the zonal current,

$$\zeta_B = [(\Delta\Theta - LGC)/\Delta\Theta]^{c_p/R}, \quad (14)$$

and $\delta\Theta$ does not enter the analysis. This case corresponds to the diagnostic analysis discussed by Smith *et al.* (1982). They consider the results for the two choices of $\Delta\Theta = 0.4\Theta(E)$ and $\Delta\Theta = 0.04\Theta(E)$. Figure 5 displays the continuous dependence of the required value for ζ_B as a function of $\Delta\Theta$ converted to dimensional units assuming $p_T = 350$ mb. The associated depth Δz (in km) for the equatorial flow is given from equations (3) and (4) as $\Delta z = c_p\Theta(E)[\zeta_B{}^{R/c_p}(E) - 1]/g$ and is indicated on the right side ordinate of Fig. 5, assuming $\Theta(E) = 100$ K. The solid curve corresponds to the evaluation of Eq. (14) with the value of LGC computed for the wind profile measured with respect to the radio period. The dashed curve corresponds to the evaluation of (14) with LGC computed with $\tau_{Ref} = \tau_{Radio} - 6$ min.

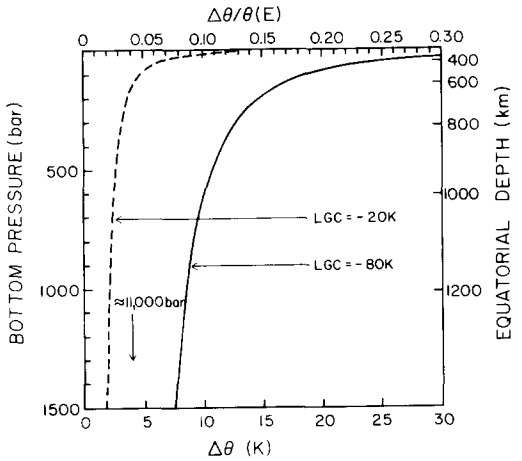

FIG. 5. Maximum depth of the zonal flow layer required to balance the inferred latitudinal geopotential contrast as a function of the horizontal potential temperature contrast. The indicated bottom pressure depth assumes a cloudtop pressure of 350 mb. The upper ordinate of the graph is labeled with the corresponding percentage difference in potential temperature, assuming $\Theta(E) = 100$°K. The solid curve corresponds to the depth for the geopotential contrast inferred from winds measured in the frame of the radio period, the dashed curve to the depth for a geopotential contrast inferred from winds in a frame with period 6 min shorter.

Case 2a. $\delta\Theta = \Delta\Theta$. (i.e., the vertical contrast across the no-motion interface at the equator equals the latitudinal contrast in the weather layer.) Then, $\zeta_B(E) = [(\Delta\Theta - LGC)/\Delta\Theta]^{c_p/R}$ as in case 1 but $\zeta_B(P)$ drops out of the balance relation. Thus, the bottom pressure for the equatorial weather layer is in this case the same function of the thermal contrast as that indicated in Fig. 5 but the bottom pressure for the weather layer at high latitudes may be arbitrarily small.

Case 2b. $\Delta\Theta = 0$. (i.e., the vertical contrast at the equator is zero.) This case is the geometric converse of case 2a, now with $\zeta_B(P) = [(\Delta\Theta - LGC)/\Delta\Theta]^{c_p/R}$ and $\zeta_B(E)$ arbitrary. This case seems less plausible than 2a, however, since for $\Delta\Theta > 0$ Eq. (11) and (12) then give $\Theta(P) < \Theta_D$, implying a convectively unstable jump between the lower and upper adiabats at the pole.

Case 3. $\zeta_B(P) \to 1$. Then the geopotential balance equation becomes

$$\zeta_B(E) = [(\delta\Theta - LGC)/\delta\Theta]^{c_p/R}, \quad (15)$$

and the horizontal thermal contrast $\Delta\Theta$ becomes irrelevant. In this extreme limit of shallow high-latitude flow, the geopotential balance is supported by the jump in potential temperature between the layers above and below $\zeta = \zeta_B(\lambda)$ with negligible contribution from the latitudinal gradient at the cloudtops. Figure 5 may still be used to evaluate the required depth of the equatorial flow, but now with $\Delta\Theta$ replaced by $\delta\Theta$ as the abscissa on the graph. (For reasons similar to our remark about case 2b, we will not consider the possibility that $\zeta_B(E) \to 1$.)

DISCUSSION

Figure 5 shows that the required bottom pressure for the zonal flow is a sensitive function of both the contrast in temperature and the bulk rotation period of the deep atmosphere. With LGC computed from the wind profile in the frame of the radio period, a 4% thermal contrast requires a bottom pressure of approximately 11,000 bars, which is comparable to the conclusion of Smith *et al.* (1982). If the bulk rotation period of the planet at depth is 6 min less than the radio period, however, the required bottom pressure is only 160 bars for a 4% contrast or 50 bars for a 6% contrast.

We have argued, however, that larger thermal contrasts cannot be ruled out by the observations. As Eq. (14) and Fig. 5 show, with $\Delta\Theta \ll$ LGC, the required bottom pressure is roughly proportional to the inverse cube of the potential temperature contrast. If the latitudinal thermal contrast is as large as 12% (with $\Delta\Theta = 12°K$), then even if the radio period is exactly the rotation period of the deep atmosphere, the maximum bottom pressure need be only 360 bars.

Furthermore, case 2a for the geopotential balance equation described in the last section demonstrates that this maximum depth need not be maintained at all latitudes. If the vertical jump in potential temperature across the no-motion interface at the equator is as large as the equator-to-pole contrast in the upper weather layer, then the depth of the flow at high latitudes is unconstrained. As discussed below, the presence of compositional gradients in Saturn's atmosphere make such vertical contrasts a real possibility. Thus, a plausible configuration for the zonal flow on Saturn is an equatorial jet extending to a few hundred bars with relatively shallow mid-to-high latitude jets extending no deeper than, for example, a few tens of bars pressure.

In the extreme limit of shallow high-latitude flow (case 3 above), the geopotential balance equation reduces to Eq. (15) for which the vertical thermal contrast across the no-motion interface is of overriding importance. If such a configuration were realized then the horizontal thermal gradients at the cloudtops would be decoupled from the dynamical balance of the zonal flow so that even with $\Delta\Theta = 0$, the observed flow could be maintained by sufficiently strong buoyancy contrasts across the latitudinally variable bottom.

There is as yet no observational basis for discriminating against one or another of these kinematic configurations. The flat-bottom case may be the simplest to model. The real structure, however, may more nearly resemble the oceanic thermocline, with strong density variations confined to levels which vary with latitude.

In every case some vertical contrast in potential temperature across the no-motion interface is required at some latitude to support the thin-layer dynamics. Clearly our understanding of the zonal flow system, if in fact it is confined to a thin upper layer, will be incomplete without a description of the physics which imposes the required buoyancy contrasts. We will not attempt to provide a definitive answer to this problem here but will mention a few possibilities and examine one in quantitative detail.

Gierasch (1983) has suggested that differentiation in the abundance of orthohydrogen and parahydrogen (cf. Massie and Hunten, 1982) may induce strong thermal gradients by the vertical transport of atmospheric parcels along different adiabats down to levels around 160 bar. Another possibility is that contrasts arise from the latent heating or differentiation of mean molecular weight associated with the condensation of atmospheric constituents. In addition to several carbon, oxygen, and nitrogen compounds, these include several hundred metallic and salt compounds. Barshay and Lewis (1978) have studied the equilibrium abundances for some 500 such compounds along the Jupiter adiabat and find that condensation of minor constituents occurs at temperatures ranging from

400 to 2000°K, corresponding to pressure depths on Saturn ranging from 40 to 10,000 bars.

One especially interesting possibility, however, is that water condensation effects may be of controlling importance for the dynamical balance of the Saturn meteorology. Barcilon and Gierasch (1970) have studied the latent heat effects for Jupiter in a steady symmetric model. Gierasch (1976) extended the predictions to the other Jovian planets and found that pre-Voyager wind speeds for Saturn could be accounted for in this way only if the planet is enriched in water abundance relative to Jupiter. Recent work on differentiated interior models for Saturn by Stevenson (1981) suggests that the IRIS observation of helium depletion (Hanel *et al.*, 1981) may be accounted for by an outer envelope which is greatly enriched in its water abundance relative to Jupiter's. According to Stevenson (private communication), the interior models require an enrichment of heavy molecules (plausibly water) in the outer envelope in order to match the measured value for Saturn's J4 gravitational moment. If the heavy species is in fact water, Stevenson's preliminary results indicate an enrichment of roughly 10 times the solar composition value.

It is possible that a feedback between the dynamics and water condensation can further enrich the moisture abundance at one latitude relative to another. We outline an estimate of water condensation pressures, thermal contrasts induced by latent heating, and the previously neglected effects of the differentiation of mean molecular weight in an appendix. Unfortunately, the uncertainties in Saturn's water abundance, the latitudinal abundance gradient, and the extent of vertical transports by precipitation and reevaporation make it impossible to obtain a unique diagnostic solution to the balance of the geopotential contrast by moisture-induced buoyancy effects. Nevertheless, the estimates given in the appendix suggest that if Saturn is enriched 10 times in water abundance relative to a solar composition atmosphere and is latitudinally differentiated so that the equatorial abundance at the condensation level is 5 times that of the interior, then the total jump in virtual temperature including latent heating effects may be sufficient to confine the flow to pressure depths less than 50 bars. (We are now assuming a reference rotation period for the bulk atmosphere equal to the radio period.) Other combinations of mean abundance and latitudinal differentiation are possible which also lead to confinement of the flow at depths comparable to the condensation pressures for the water clouds.

SUMMARY

If the bulk of the molecular hydrogen envelope of Saturn rotates as a solid body with a period which is a few minutes less than the measured radio period, the magnitude of thermal (or density) contrasts required to support the observed flow over a thin layer will be greatly reduced. With a bulk rotation period 1% less than the radio period, for example, a 5% thermal contrast will confine the zonal flow to depths less than 80 bars. Although it is not clear how such a period shift may be produced, the sensitivity of the meteorological analysis to the bulk rotation rate and the uncertainty about the real source of the kilometric radio signal used to define this rate (Warwick *et al.*, 1981) make this an important area for further consideration. Can ionospheric loading of charged particles cause the signal rate to shift with respect to the rotation rate of the frozen-in field lines? Can deep interior currents cause the magnetic field to drift rapidly to the west with respect to the molecular envelope? Both magnetospheric theory and models of the magnetic dynamo may be of relevance here.

Even if the bulk rotation period is exactly the radio period, the required depth for the flow is still a sensitive function of the thermal contrast at levels below the cloud tops. The IRIS measurements cannot give a reliable upper limit on thermal gradients at

these depths (although there is some indication of differential solar heating above). Further radiative–convective modeling of clouds and aerosols in Jovian atmospheres might be of value in assessing the effects of absorbed sunlight at depth.

We have shown that the situation might be complicated by a thin-layer configuration with a lower level of no motion which varies with latitude. Saturn's strong equatorial jet may lie at deeper levels than the high-latitude flow. Then vertical buoyancy contrasts across the no-motion interface could be as important as the horizontal contrast between equator and pole.

Compositional gradients may play a controlling role in both the vertical and horizontal contrasts. We have shown in the Appendix that if Saturn's envelope is greatly enriched in water abundance relative to a solar composition atmosphere and strongly differentiated with latitude, then moisture condensation effects could by themselves provide the required gradients for a zonal flow confined to the vicinity of the cloud layer. It would be of interest to extend these crude estimates with chemical equilibrium computations as careful and complete as those of Weidenschilling and Lewis (1973) both for a water-enriched cloud layer and for the deeper cloud layers associated with the metallic and salt compounds. Observational measurements of abundance gradients would be welcome but are probably difficult to obtain at depth. De Pater and Dickel (1982) have shown that radio maps of Saturn at wavelengths close to 1 cm from the very large array (VLA) give equal limb darkening in both the north–south and east–west directions only if the ammonia abundance decreases with latitude. It would be of great interest to see if the VLA measurements could also be applied to modeling of the water abundance.

The observational uncertainties and alternative configurations for thin-layer flows described in this study make it impossible to rule out an entire class of Saturn atmospheric models by diagnostic analysis of cloud-tracked winds. The analysis of Smith *et al.* (1982) has demonstrated the need to reexamine previous ideas about Jovian meteorology in the light of new observations. It remains to be seen, however, whether the real flow on Saturn (and Jupiter) is confined to a thin upper layer or extends completely through the envelope in counterrotating cylinders. Our understanding of the Saturn meteorology will ultimately require detailed solutions of the time-dependent equations of motion coupled to realistic models of the thermodynamics for further comparison with the observations.

APPENDIX: MOISTURE CONDENSATION EFFECTS

Recent modeling of the Saturn interior by Stevenson (1981) suggests that the outer envelope may be greatly enriched in some heavy molecular species (plausibly water) relative to Jupiter's atmosphere. If this species is in fact water, then preliminary computations (Stevenson, private communication) indicate an enrichment amounting to roughly 10 times the solar composition value. Such a large water abundance implies the possibility of strong buoyancy contrasts at the water condensation level, owing both to latent heat release and the differentiation of mean molecular weight.

In order to obtain a quantitative estimate of these effects we will assume that in the final steady state the moist convection assumes a configuration which may be analyzed according to an admittedly crude and somewhat speculative recipe based on simple thermodynamic arguments and an idealized geometry. It is not our purpose here to prescribe the feedback between vertical velocity and diabatic heating (as in terrestrial cumulus parameterization) but only to estimate the possible magnitude of temperature (and density) contrasts as they apply to the diagnostic analysis of the geostrophic flow.

We assume that moisture condenses within a very thin layer (compared with the depth of the zonal flow) just above the no-motion interface separating the upper

weather system from the deep atmosphere (cf. Fig. 4). Within this very thin layer, which we will call the condensation interface, the mass mixing ratio for the water vapor, denoted by X, is latitudinally differentiated so that $X = X(\lambda)$. We will assume that the differentiation works in a way to make the equatorial mixing ratio, $X(\mathrm{E})$, greater than the value for X at higher latitudes. At deep levels below the interface, however, $X = X_D$ a constant as required by the assumption that the deep atmosphere be effectively isentropic (as far as the zonal dynamics is concerned).

The quantitative estimate of condensation pressures, latent heating, and differentiation of mean molecular weight are then derived from the following additional assumptions.

(1) The potential temperature just above the condensation interface is warmer due to latent heat release than that at deeper levels in proportion to the local mass mixing ratio of water on the interface X by an amount

$$\delta\Theta^L = \zeta_c^{-R/c_p} LX/c_p \cong \zeta_c^{-R/c_p} (X/X_\odot)(1.67°\mathrm{K}) \quad \text{(A1)}$$

(cf. Barcilon and Gierasch, 1970). Here $L = 2.5 \times 10^{10}$ cm^2 sec^{-2} denotes the latent heat of vaporization of water, ζ_c denotes the (nondimensional) pressure level for the condensation (assumed coincident with the no-motion interface ζ_B), and $X_\odot = 8.83 \times 10^{-3}$ is the mass mixing ratio of water vapor for a solar composition atmosphere (grams of vapor per grams of dry air).

(2) Since the latent heat effects and the associated jump in potential temperature are assumed greatest at the equator, the upper layer adiabat there is displaced from the deep isentropic adiabat according to the relation

$$\Theta(\mathrm{E}) = \Theta_D + \delta\Theta^L(\mathrm{E}). \quad \text{(A2)}$$

(3) The moisture condensation pressure coincides with the level where the water vapor pressure equals the saturation vapor pressure given by the Clausius–Clapeyron equation. After expressing the vapor pressure in terms of the mass mixing ratio X, the condensation pressure is therefore determined by

$$\zeta_c \cong X^{-1} p_T^{-1} e_0 (m_v/m_d) \exp\left[\left(\frac{1}{273°\mathrm{K}} - \frac{1}{\Theta_D \zeta_c^{R/c_p}}\right) m_v L/R^*\right], \quad \text{(A3)}$$

solved simultaneously with Eqs. (A1) and (A2). Here $e_0 = 0.00611$ bar is the saturation vapor pressure at 273°K, $m_v = 18$ g mol^{-1} is the molecular weight of water, $m_d = 2.14$ g mol^{-1} is the molecular weight of dry (hydrogen–helium) air, and $R^* = 8.317 \times 10^7$ erg mol^{-1} °K^{-1} is the universal gas constant.

(4) The differentiation of mean molecular weight between the dry upper layer and the lower vapor layer introduces a jump in the gas constant which may be expressed as a jump in "virtual temperature" (defined so that the same value for R may be retained in the dynamic equations at all locations). Since moist air is heavier than dry hydrogen–helium air, the vapor layer will have a "colder" virtual temperature than the layer above. The contrast is simply computed from the mixing ratio and molecular weight ratio as

$$\delta\Theta^v = \Theta(1 - m_d/m_v)X/(1 + X) \quad \text{(A4)}$$

(5) Now the total vertical jump $\delta\tilde{\Theta}$ in the virtual potential temperature (including latent heating) across the condensation interface at the equator is evaluated with $X = X(\mathrm{E})$ in Eq. (A1) and $X = X_D$ in Eq. (A4), i.e.,

$$\delta\tilde{\Theta} = \delta\Theta^L|_{X=X(\mathrm{E})} + \delta\Theta^v|_{X=X_D}. \quad \text{(A5)}$$

(6) In order to apply these estimates in the simplest possible way we will further suppose that the zonal wind layer assumes the extreme limit of shallow high-latitude flow discussed above as special case 3 for the geopotential balance equation (with $\zeta_B(\mathrm{P}) \to 1$). If the condensation interface is in fact coincident with the no-motion level, such a configuration may result from the

depletion of condensed water on this interface at the pole, so that $X(P) \to 0$.

With these assumptions and the understanding that the total virtual temperature variation $\delta\tilde{\Theta}$ now acts in the same way as $\delta\Theta$ in Eq. (15), we may apply the results of Eq. (A5) to the relation between thermal contrast and pressure depth shown in Fig. 5. (We will assume for now that Saturn's bulk rotation period is exactly the radio period but will recall that if it is a few minutes shorter, the thermal contrast requirements for a thin layer will be much less severe.)

Table AI gives the indicated condensation pressure and associated changes in potential and virtual temperature for different values of the mass mixing ratio (in multiples of the solar composition value $X_\odot$) according to the prescription of Eqs. (A1)–(A4) above. The table is extended to $X/X_\odot = 50$ to allow for the possibility that large mean abundances for the outer envelope (with $X_D \approx 10\ X_\odot$?) may be further enriched (up to five times, for example) by horizontal differentiation at the condensation interface.

Table AII then summarizes an application of these results to an evaluation of the total jump in virtual potential temperature prescribed by Eq. (A5) for different values of X_D and the latitudinal differentiation factor $X(E)/X_D$. The corresponding value of the required bottom pressure may then be obtained from Eq. (15) and Fig. 5. In order for water condensation effects to be a plausible candidate for the required buoyancy contrasts the indicated pressure depth must be in the vicinity of the condensation levels. (The numbers in Table AI might be a slight underestimate of the pressure depth of cloud induced gradients in the presence of strong precipitation. Rossow (1978) has shown that on Jupiter precipitating water droplets may fall half a scale height before they are reevaporated.) Because of uncertainties in vertical transports and the actual values for the Saturn water abundance, it is impossible to obtain a unique solution to the diagnostic analysis of water condensation. The results in Table AII do suggest, however, that unless X_D is as large as 20 $X_\odot$, strong latitudinal differentiation on the condensation interface is required to produce a large enough value for $\delta\tilde{\Theta}$ to restrict the flow to cloud condensation depths in this way.

With $X_D = 10\ X_\odot$ and $X(E)/X_D = 5$ (so that the equatorial condensation depth is close to 80 bars), the indicated jump in total virtual temperature is around 24°K. Figure 5 shows that the corresponding depth for a confined upper layer flow is around 50 bars. This combination of mean envelope abundance and latitudinal differentiation is therefore a plausible configuration for the support of a thin-layer flow. By a similar process of inspection, Table AII shows that another plausible configuration corresponds to the parameter setting $X_D = 20\ X_\odot$ and $X(E)/X_D = 2$.

TABLE AI

MOISTURE CONDENSATION PARAMETERS

$X/X_\odot$	Condensation pressure (bar)	$\delta\Theta^L$ (°K)	$\delta\Theta^v$ (°K)
1	12	0.6	0.8
2	15	1.1	1.5
5	20	2.6	3.7
10	26	4.7	7.2
20	38	8.4	13.2
50	78	17.0	27.0

TABLE AII

THE TOTAL JUMP IN VIRTUAL POTENTIAL TEMPERATURE (INCLUDING LATENT HEATING)
$\delta\tilde{\Theta} = \delta\Theta^L|_{X=X(E)} + \delta\Theta^v|_{X=X_D}$

$X(E)/X_D$	1	2	5
$X_D/X_\odot$			
1	1.4	1.9	3.4
5	6.3	8.4	13.8
10	11.9	15.6	24.2
20	21.6	27.7	39.9

ACKNOWLEDGMENTS

We are grateful to B. J. Conrath, A. Del Genio, L. Travis, and W. Rossow for useful discussions of this

work. We also thank A. P. Ingersoll and an anonymous referee for their helpful reviews. M. Allison is supported by the National Research Council as a Resident Research Associate at NASAs Goddard Institute for Space Studies in New York.

REFERENCES

BARCILON, A., AND P. GIERASCH (1970). A moist, Hadley cell model for Jupiter's cloud bands. *J. Atmos. Sci.* **27,** 550–560.

BARSHAY, S. S., AND J. S. LEWIS (1978). Chemical structure of the deep atmosphere of Jupiter. *Icarus* **33,** 593–611.

BUSSE, F. H. (1976). A simple model of convection in the Jovian atmosphere. *Icarus* **29,** 255–260.

CONRATH, B. J., P. J. GIERASCH, AND N. NATH (1981). Stability of zonal flows on Jupiter. *Icarus* **48,** 256–282.

CONRATH, B. J., AND J. A. PIRRAGLIA (1983). Thermal structure of Saturn from Voyager infrared measurements: Implications for atmospheric dynamics. *Icarus* **53,** 286–292.

COSPAR (1972). *COSPAR International Reference Atmosphere (CIRA)*. Akademie-Verlag, Berlin.

DE PATER, I., AND J. R. DICKEL (1982). VLA observations of Saturn at 1.3, 2, and 6 cm. *Icarus* **50,** 88–102.

DESCH, M. D., AND KAISER, M. L. (1981). Voyager measurement of the rotation period of Saturn's magnetic field. *Geophys. Res. Lett.* **8,** 253–256.

GIERASCH, P. J. (1976). Jovian meteorology: Large-scale moist convection. *Icarus* **29,** 445–454.

GIERASCH, P. J. (1983). Dynamical consequences of orthohydrogen-parahydrogen disequilibrium on Jupiter and Saturn. *Science* **219,** 847–849.

GIERASCH, P. J., AND R. M. GOODY (1969). Radiative time constants in the atmosphere of Jupiter. *J. Atmos. Sci.* **26,** 979–980.

HANEL, R., B. CONRATH, F. M. FLASER, V. KUNDE, W. MAGUIRE, J. PEARL, J. PIRRAGLIA, R. SAMUELSON, L. HERATH, M. ALLISON, D. CRUIKSHANK, D. GAUTIER, P. GIERASCH, L. HORN, R. KOPPANY, AND C. PONNAMPERUMA (1981). Infrared observations of the Saturnian system from Voyager 1. *Science* **212,** 192–200.

INGERSOLL, A. P. (1976). Pioneer 10 and 11 observations and the dynamics of Jupiter's atmosphere. *Icarus* **29,** 245–253.

INGERSOLL, A. P., AND D. POLLARD (1982). Motion in the interiors and atmospheres of Jupiter and Saturn: Scale analysis, anelastic equations, barotropic stability criterion, *Icarus* **52,** 62–80.

INGERSOLL, A. P., R. F. BEEBE, J. L. MITCHELL, G. W. GARNEAU, G. M. YAGI, AND J. MULLER (1981). Interactions of eddies and mean zonal flow on Jupiter as inferred from Voyager 1 and 2 images. *J. Geophys. Res.* **86,** 8733–8743.

KAISER, M. L., M. D. DESCH, AND A. LECACHEUX (1981). Saturnian kilometric radiation: statistical properties and beam geometry. *Nature* **292,** 731–733.

MASSIE, S. T., AND HUNTEN, D. M. (1982). Conversion of *para* and *ortho* hydrogen in the Jovian planets. *Icarus* **49,** 213–226.

NITANI, H. (1972). Beginning of the Kuroshio. In *Kuroshio: Physical Aspects of the Japan Current* (H. Stommel and K. Yoshida, Eds.), pp. 129–163. University of Washington Press, Seattle.

PIRRAGLIA, J. A., B. J. CONRATH, M. D. ALLISON, AND P. J. GIERASCH (1981). Thermal structure and dynamics of Saturn and Jupiter *Nature* **292,** 677–679.

ROSSOW, W. B. (1978). Cloud microphysics: Analysis of the clouds of Earth, Venus, Mars, and Jupiter. *Icarus* **36,** 1–50.

SMITH, B. A., L. SODERBLOM, R. BATSON, P. BRIDGES, J. INGE, H. MASURSKY, E. SHOEMAKER, R. BEEBE, J. BOYCE, G. BRIGGS, A. BUNKER, S. A. COLLINS, C. J. HANSEN, T. V. JOHNSON, J. L. MITCHELL, R. J. TERRILE, A. F. COOK, J. CUZZI, J. B. POLLACK, G. E. DANIELSON, A. P. INGERSOLL, M. E. DAVIES, G. E. HUNT, D. MORRISON, T. OWEN, C. SAGAN, J. VEVERKA, R. STROM, AND V. E. SUOMI (1982). A new look at the Saturn system: The Voyager 2 images. *Science* **215,** 504–537.

STEVENSON, D. J. (1981). New models of Jupiter and Saturn: Contrasting interiors? *Bull. Amer. Astron. Soc.* **13,** 740.

STONE, P. H. (1972). A simplified radiative-dynamical model for the static stability of rotating atmospheres. *J. Atmos. Sci.* **29,** 405–418.

STONE, P. H. (1976). The meteorology of the Jovian atmosphere. In *Jupiter* (T. Gehrels, Ed.), pp. 586–618. Univ. of Arizona Press, Tucson.

WARWICK, J. W., J. B. PEARCE, D. R. EVANS, T. D. CARR, J. J. SCHAUBLE, J. K. ALEXANDER, M. L. KAISER, M. D. DESCH, M. PEDERSON, A. LECACHEUX, G. DAIGNE, A. BOISCHOT, AND C. H. BARROW (1981). Planetary radio astronomy observations from Voyager 1 near Saturn. *Science* **212,** 239–243.

WEST, R. A. (1983). Spatially resolved methane band photometry of Saturn. II. Cloud structure models at four latitudes. *Icarus* **53,** 301–309.

WEIDENSCHILLING, S. J., AND J. S. LEWIS (1973). Atmospheric and cloud structures of the Jovian planets. *Icarus* **20,** 465–476.